

Article

# Synthesis, Structures, Electrochemistry, and Catalytic Activity towards Cyclohexanol Oxidation of Mono-, Di-, and Polynuclear Iron(III) Complexes with 3-Amino-2-Pyrazinecarboxylate

Anirban Karmakar <sup>1,\*</sup> , Luísa M.D.R.S. Martins <sup>1,\*</sup> , Yuliya Yahorava <sup>2</sup>,  
M. Fátima C. Guedes da Silva <sup>1</sup>  and Armando J. L. Pombeiro <sup>1,\*</sup>

<sup>1</sup> Centro de Química Estrutural, Instituto Superior Técnico, Universidade de Lisboa, Av. Rovisco Pais, 1049-001 Lisbon, Portugal; fatima.guedes@tecnico.ulisboa.pt

<sup>2</sup> Department of Chemistry, Technology of Electrochemical Production and Electronic Engineering Materials, Belarusian State Technological University, 13a Sverdlova str., 220006 Minsk, Belarus; egorova.y\_a@mail.ru

\* Correspondence: anirbanchem@gmail.com (A.K.); luisammartins@tecnico.ulisboa.pt or luisamargaridamartins@tecnico.ulisboa.pt (L.M.D.R.S.M.); pombeiro@tecnico.ulisboa.pt (A.J.L.P.)

Received: 20 March 2020; Accepted: 9 April 2020; Published: 13 April 2020



**Abstract:** The synthesis and characterization of a set of iron(III) complexes, viz. the mononuclear [Fe(L)<sub>3</sub>] (**1**) and [NH<sub>4</sub>][Fe(L)<sub>2</sub>(Cl)<sub>2</sub>] (**2**), the dinuclear methoxido-bridged [Fe(L)<sub>2</sub>(μ-OMe)]<sub>2</sub>.DMF.1.5MeOH (**3**), and the heteronuclear Fe(III)/Na(I) two-dimensional coordination polymer [Fe(N<sub>3</sub>)(μ-L)<sub>2</sub>(μ-O)<sub>1/2</sub>(Na)(μ-H<sub>2</sub>O)<sub>1/2</sub>]<sub>n</sub> (**4**), are reported. Reactions of 3-amino-2-pyrazinecarboxylic acid (HL) with iron(III) chloride under different reaction conditions were studied, and the obtained compounds were characterized by elemental analysis, Fourier Transform Infrared (FT-IR) spectroscopy, and X-ray single-crystal diffraction. Compound **1** is a neutral mononuclear complex, whereas **2** is mono-anionic with its charge being neutralized by triethylammonium cation. Compounds **3** and **4** display a di-methoxido-bridged dinuclear complex and a two-dimensional heterometallic Fe(III)/Na(I) polynuclear coordination polymer, respectively. Compounds **3** and **4** are the first examples of methoxido- and oxido-bridged iron(III) complexes, respectively, with 3-amino-2-pyrazinecarboxylate ligands. The electrochemical study of these compounds reveals a facile single-electron reversible Fe(III)-to-Fe(II) reduction at a positive potential of 0.08V vs. saturated calomel electrode (SCE), which is in line with their ability to act as efficient oxidants and heterogeneous catalysts for the solvent-free microwave-assisted peroxidative oxidation (with *tert*-butyl hydroperoxide) of cyclohexanol to cyclohexanone (almost quantitative yields after 1 h). Moreover, the catalysts are easily recovered and reused for five consecutive cycles, maintaining a high activity and selectivity.

**Keywords:** Iron(III) complex; Crystal structure; Electrochemistry; Catalysis; Oxidation reaction

## 1. Introduction

The coordination chemistry of iron(III) compounds with oxido-bridged species is valuable to synthetic chemists [1] namely due of their applications in biological systems, such as in storage and transport of dioxygen [2], phosphate ester hydrolysis [3], DNA synthesis [4], etc. Moreover, oxido-bridged dinuclear iron(III) units are also present at the active site of various non-heme metalloenzymes, such as hemerythrin, methane monooxygenase (MMO), ribonucleotide reductase, etc. [5]. Several oxido- [6], hydroxido- [7], alkoxido- [8], peroxido- [9], or carboxylato-bridged [10] iron(III) complexes or coordination polymers have been reported by various research groups, which show interesting applications in areas of magnetism, catalysis, biology, electrochemistry, etc. [11].

On the other hand, pyrazine-based carboxylate ligands are important building blocks for the construction of various complexes and coordination polymers due to their versatile metal-binding and hydrogen-bonding capabilities [12]. 2-Pyrazinecarboxylate is illustrative of such behaviors [13]; moreover, by introducing substituents into the pyrazine ring, we can modify its coordination and hydrogen bonding properties. In this context, we have chosen an amine-substituted pyrazine carboxylate ligand, namely 3-aminopyrazine-2-carboxylic acid (HL), which has a good propensity for the formation of coordination and hydrogen bonds, as well as for  $\pi$ - $\pi$  stacking interactions. It is known to form complexes with s-block [14], d-block [15], and f-block [16] metal ions. Moreover, our group has also reported several Sn(II), Pb(II), and Fe(III) metal complexes and coordination polymers based on such a ligand, and studied their polymorphic and catalytic activity towards some organic transformations [17–19]. Although a few oxido and methoxido iron complexes are known [9,20], no example of oxido- or methoxo-bridged Fe(III) complexes with 3-aminopyrazine-2-carboxylic acid has been reported. Thus, the synthesis and study of complexes of this type constitute the general aim of the current work.

The oxidation of alcohols to carbonyl compounds is one of the significant reactions in organic chemistry, and many metal-based homogeneous catalysts have been developed [21]. However, most of these systems required harsh reaction conditions, metal and solvent toxicity, high cost, or high reagent load or produced unwanted waste. To remove the harmful wastes, the development of catalytic oxidation procedures which involve green methods is a matter of current interest [22] and, in this context, microwave-assisted solvent-free oxidation of alcohols using environmentally suitable and effective catalyst, which can operate under mild conditions, are of a particular interest [23].

Besides that, iron is mostly used in many oxidation reactions, such as epoxidation [24], sulfoxidation [25], hydroxylation [26], etc. Alcohol oxidations are also catalyzed by iron complexes, and examples have been reported by our group, namely concerning the oxidations of secondary alcohols and cycloalkanes under microwave (MW) irradiation [27,28]. Besides, the dichloro hydrotris (pyrazol-1-yl)methane iron(II) complex, heterogenized on carbon materials or zeolites or dispersed in ionic liquids, in the presence of 2-pyrazinecarboxylic acid, is an active, selective, and recyclable catalyst for oxidation of cyclohexane [29]. In addition, 2-pyrazinecarboxylic acid is an additive in the oxidation of alkanes catalyzed by iron(III) complexes [30]. Thus, heterogeneous catalytic systems based on substituted pyrazinecarboxylic acid-Fe(III) species should be promising for an efficient, clean, and safe alcohol oxidation reaction.

Hence, we report herein the synthesis and structural characterization of a set of iron(III) complexes, viz. the mononuclear  $[\text{Fe}(\text{L})_3]$  (1) and  $[\text{NHEt}_3][\text{Fe}(\text{L})_2(\text{Cl})_2]$  (2), the dinuclear methoxido-bridged  $[\text{Fe}(\text{L})_2(\mu\text{-OMe})_2]\cdot\text{DMF}\cdot 1.5\text{MeOH}$  (3), and the heteronuclear Fe(III)/Na(I) two-dimensional coordination polymer  $[\text{Fe}(\text{N}_3)(\mu\text{-L})_2(\mu\text{-O})_{1/2}(\text{Na})(\mu\text{-H}_2\text{O})_{1/2}]_n$  (4) (HL = 3-amino-2-pyrazinecarboxylic acid). Their heterogeneous catalytic performance was tested towards solvent-free peroxidative oxidation (under focused MW irradiation) of cyclohexanol to cyclohexanone, which concerns an industrially important step for polyamide 6 production [31].

## 2. Experimental

The synthetic work was performed in air. All the chemicals were obtained from commercial sources and used as received. The infrared spectra ( $4000\text{--}400\text{ cm}^{-1}$ ) were recorded on a Bruker Vertex 70 instrument in KBr pellets; abbreviations: s = strong, m = medium, w = weak, bs = broad and strong, mb = medium and broad. Carbon, hydrogen, and nitrogen elemental analyses were carried out by the Microanalytical Service of the Instituto Superior Técnico.

### 2.1. Synthesis of 1

To a hot and stirred ethanolic suspension (10 mL) of 3-amino-2-pyrazinecarboxylic acid (0.28 g, 2 mmol), an ethanolic solution (5 mL) of  $\text{FeCl}_3\cdot 6\text{H}_2\text{O}$  (0.27 g, 1 mmol) was added dropwise to produce a dark red solution. The mixture was refluxed for 2 h and kept for slow evaporation. After 3 days, the

red crystalline compound containing diffractable crystals was collected by filtration and washed with methanol. Yield: 71% based on Fe. Anal. Calcd. for  $C_{15}H_{12}FeN_9O_6$  ( $M = 470.19$ ): C, 38.32; H, 2.57; N, 26.81; Found: C, 38.43; H, 2.41; N, 26.18. FT-IR (KBr,  $cm^{-1}$ ): 3456 (bs), 3393 (bs), 3145 (bs), 1612 (s), 1558 (m), 1440 (m), 1368 (s), 1325 (s), 1230 (s), 1189 (s), 1149 (s), 1030 (m), 922 (s), 835 (s), 819 (s), 721 (m), 526 (s), 448 (s).

## 2.2. Synthesis of 2

The mixture of  $FeCl_3 \cdot 6H_2O$  (0.27 g, 1 mmol) and 3-amino-2-pyrazinecarboxylic acid (0.28 g, 2 mmol) was dissolved in 15 mL of methanol. The resulting solution was stirred at room temperature and triethylamine (0.10 g, 1 mmol) was then added. The mixture was kept under stirring for 4 h at room temperature. After 2 days, the red crystalline compound containing diffractable crystals was collected by filtration and washed with methanol. Yield: 89% based on Fe. Anal. Calcd. For  $C_{16}H_{24}Cl_2FeN_7O_4$  ( $M = 505.17$ ): C, 38.04; H, 4.79; N, 19.41; Found: C, 38.23; H, 4.61; N, 19.18. FT-IR (KBr,  $cm^{-1}$ ): 3442 (bs), 3208 (bs), 2978 (m), 2734 (m), 1625 (s), 1604 (s), 1545 (m), 1483 (m), 1476 (m), 1458 (m), 1365 (s), 1339 (m), 1232 (m), 1148 (m), 1029 (w), 928 (m), 850 (m), 831 (m), 672 (s), 641 (m), 534 (m).

## 2.3. Synthesis of 3

The mixture of  $FeCl_3 \cdot 6H_2O$  (0.27 g, 1 mmol) and 3-amino-2-pyrazinecarboxylic acid (0.42 g, 3 mmol) was dissolved in 15 mL of a mixture of DMF and methanol (1:1) and kept stirred at room temperature for 6 h. The resulting solution was left for slow evaporation, and after 7 days, red-plates like crystals formed, were collected by filtration, and washed with methanol. Yield: 73% based on Fe. Anal. Calcd. For  $C_{26.5}H_{35}Fe_2N_{13}O_{12.5}$  ( $M = 847.33$ ): C, 37.56; H, 4.16; N, 21.49; Found: C, 37.23; H, 4.21; N, 21.28. FT-IR (KBr,  $cm^{-1}$ ): 3462 (bs), 3389 (bs), 3280 (bs), 1737 (s), 1688 (m), 1654 (m), 1609 (s), 1563 (w), 1543 (w), 1443 (m), 1401 (s), 1367 (s), 1322 (m), 1297 (m), 1232 (m), 1188 (s), 1154 (s), 1001 (w), 924 (w), 818 (s), 695 (m), 677 (m), 561 (s).

## 2.4. Synthesis of 4

The mixture of  $FeCl_3 \cdot 6H_2O$  (0.27 g, 1 mmol), 3-amino-2-pyrazinecarboxylic acid (0.28 g, 2 mmol), and  $NaN_3$  (0.06 g, 1 mmol) was dissolved in 4 mL of a 1:1 mixture of DMF and MeOH. The resulting solution was sealed in a vessel and heated at 75 °C for 48 h. It was subsequently cooled to room temperature (0.2 °C  $min^{-1}$ ), affording block-type reddish crystals. Yield: 61% based on Fe. Anal. Calcd. for  $C_{10}H_9FeN_9NaO_5$  ( $M = 414.10$ ): C, 29.01; H, 2.19; N, 30.44; Found: C, 29.65; H, 2.11; N, 30.08. FT-IR (KBr,  $cm^{-1}$ ): 3466 (bs), 3397 (bs), 3342 (bs), 3107 (bs), 1652 (s), 1600 (m), 1548 (m), 1462 (w), 1438 (m), 1356 (s), 1319 (m), 1240 (m), 1202 (s), 1141 (s), 1021 (m), 924 (s), 835 (s), 819 (s), 732 (w), 696 (m), 602 (m), 548 (m), 449 (s).

## 2.5. Electrochemical Studies

The electrochemical experiments were performed on an EG&G PAR 273A potentiostat/galvanostat connected to a personal computer through a GPIB interface. Cyclic voltammetry (CV) studies were undertaken in 0.2 M [ $nBu_4N$ ][ $BF_4$ ]/DMSO, at a platinum disc working electrode ( $d = 0.5$  mm) and at room temperature. Controlled-potential electrolysis (CPE) was carried out in electrolyte solutions with the above-mentioned composition, in a three-electrode H-type cell. The compartments were separated by a sintered glass frit and equipped with platinum gauze working and counter electrodes. For both CV and CPE experiments, a Luggin capillary connected to a silver wire pseudo-reference electrode was used to control the working electrode potential. A Pt wire was employed as the counter-electrode for the CV cell. The CPE experiments were monitored regularly by CV, thus assuring no significant potential drift occurred along the electrolysis. The solutions were saturated with  $N_2$  by bubbling this gas before each run, the redox potentials of the complexes were measured by CV in the presence of ferrocene as the internal standard, and their values are quoted relative to the SCE by using the  $[Fe(\eta^5-C_5H_5)_2]^{0/+}$  redox couple [32].

## 2.6. Crystal Structure Determinations

X-ray quality single crystals of the compounds were immersed in cryo-oil, mounted in a nylon loop and measured at room temperature (1–4). Intensity data were collected using a Bruker APEX-II PHOTON 100 diffractometer with graphite monochromated Mo-K $\alpha$  ( $\lambda$  0.71069) radiation. Data were collected using phi and omega scans of 0.5° per frame, and a full sphere of data was obtained. Cell parameters were retrieved using Bruker SMART [33–35] software and refined using Bruker SAINT [33] on all the observed reflections. Absorption corrections were applied using SADABS. [33] Structures were solved by direct methods by using the SHELXS-97 package [34] and refined with SHELXL-97 [34]. Calculations were performed using the WinGX System–Version 1.80.03 [35]. The hydrogen atoms attached to carbon atoms and to the nitrogen atoms were inserted at geometrically calculated positions and included in the refinement using the riding-model approximation; Uiso(H) were defined as 1.2Ueq of the parent nitrogen atoms or the carbon atoms for phenyl and methylene residues, and 1.5Ueq of the parent carbon atoms for the methyl groups and O atom of the water ligand. Least square refinements with anisotropic thermal motion parameters for all the non-hydrogen atoms and isotropic ones for the remaining atoms were employed.

Compounds 2 contained disordered non-coordinated DMF molecules which could not be modelled reliably. PLATON/SQUEEZE [36] was used to correct the data and potential volumes of 333 Å<sup>3</sup> was found with 88 electrons per unit cell worth of scattering. The electron count suggests the presence of approximately one DMF molecule per asymmetric unit. Elemental analytical data also support this result. These were removed from the model and not included in the empirical formula. Crystallographic data are summarized in Table S1 (Supplementary Materials), and selected bond distances and angles are presented in Table S2. The hydrogen bonding interactions in compounds 1–4 are presented in Table S3. CCDC files 1991732–1991735, respectively, contain the supplementary crystallographic data for this paper. These data can be obtained free of charge from The Cambridge Crystallographic Data Centre via [www.ccdc.cam.ac.uk/data\\_request/cif](http://www.ccdc.cam.ac.uk/data_request/cif).

## 2.7. General Procedure for the Peroxidative Oxidation of Cyclohexanol

The catalytic tests under microwave irradiation (MW) were performed in a focused Anton Paar Monowave 300 microwave reactor using a 10 mL capacity reaction tube with a 13 mm internal diameter, fitted with a rotational system and an infrared (IR) temperature detector. Cyclohexanol (5 mmol), *tert*-butyl hydroperoxide (TBHP, 70% aqueous solution, 10 mmol) and 1–4 (1–10  $\mu$ mol, 0.02–0.2 mol% vs. substrate, i.e., 1, 3, 5, and 10  $\mu$ mol of each compounds 1–4) were introduced in the tube and placed in the microwave reactor. In the experiments with radical traps, CBrCl<sub>3</sub> or NHPPh<sub>2</sub> (5 mmol) was added to the reaction mixture. The system was stirred and irradiated (10–50 W) for 0.5–3 h at 60–80 °C. After the reaction, the mixture was allowed to cool to room temperature, and 150  $\mu$ L of benzaldehyde (internal standard) and 5 mL of CH<sub>3</sub>CN were added. The obtained mixture was stirred for approximately 15 min, filtered, and then a sample (1  $\mu$ L) was taken from the organic phase and analyzed by gas chromatography (GC). Chromatographic analyses were undertaken by using a Fisons Instruments GC 8000 series gas chromatograph with a DB-624 (J&W) capillary column (DB-WAX, column length: 30 m; internal diameter: 0.32 mm), flame ionization detector (FID) detector, and the Jasco Borwin v.1.50 software. The temperature of injection was 240 °C. The initial temperature was maintained at 140 °C for 1 min, then raised 10 °C/min to 220 °C and held at this temperature for 1 min. Helium was used as the carrier gas. The internal standard method was used to quantify (the result of two concordant assays) the organic products. In some cases the oxidation products were also identified by the hyphenated gas chromatography–mass spectrometry (GC-MS) technique using a Perkin Elmer Clarus 600 gas chromatograph, equipped with two capillary columns (SGE BPX5; 30 m  $\times$  0.32 mm  $\times$  25 mm), one having an EI (electron impact)-MS detector and the other a FID detector. Helium was used as the carrier gas. Reaction products were identified by comparison of their retention times with known reference compounds, and by comparing their mass spectra to fragmentation patterns obtained

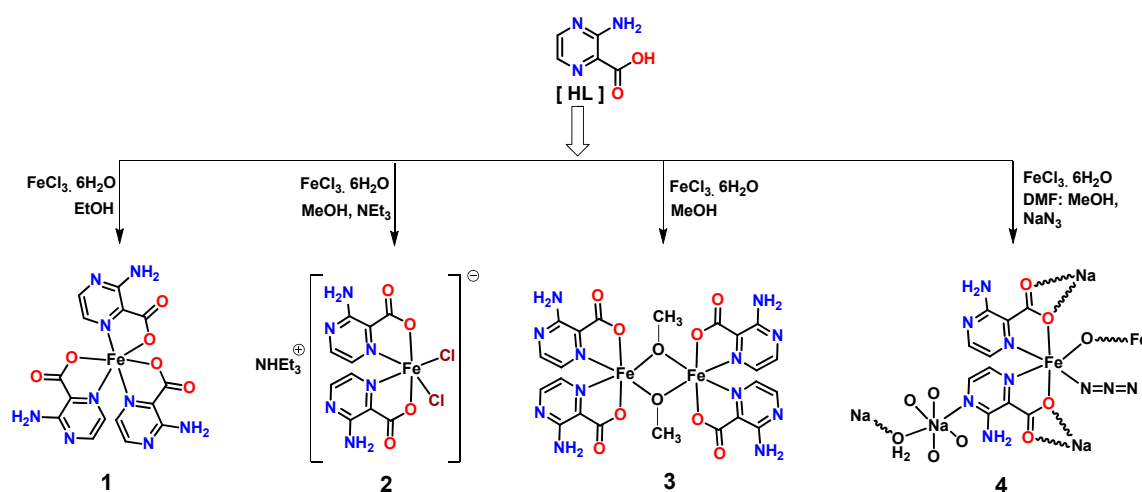
from the NIST spectral library stored in the computer software of the mass spectrometer. Blank tests indicate that only 7% of the ketones are generated in a metal-free system.

Recyclability of catalyst **3**, the one with the highest catalytic activity, was investigated for up to six cycles. Each run was initiated after the preceding one upon addition of new typical portions of all reagents. After completion of each run, the products were analyzed as mentioned above, and the catalyst was recovered by filtration of the supernatant solution after centrifugation, thoroughly washed with several portions of CH<sub>3</sub>CN, and dried overnight in an oven at 80 °C.

### 3. Results and Discussion

#### 3.1. Syntheses and Characterization

The reaction of 3-amino-2-pyrazinecarboxylic acid (HL) with iron(III) chloride hexahydrate in ethanol under reflux leads to the formation of the mononuclear [Fe(L)<sub>3</sub>] (**1**) (L = 3-amino-2-pyrazinecarboxylate). The syntheses of [NHEt<sub>3</sub>][Fe(L)<sub>2</sub>(Cl)<sub>2</sub>] (**2**) and [Fe(L)<sub>2</sub>(μ-OMe)]<sub>2</sub>.DMF.1.5MeOH (**3**) were carried at room temperature, by reacting HL with iron(III) chloride hexahydrate in the presence or absence of triethylamine in MeOH (Scheme 1). Moreover, the solvothermal reaction of HL with FeCl<sub>3</sub>.6H<sub>2</sub>O in the presence of NaN<sub>3</sub> in DMF and methanol mixture leads to the formation of the 2D oxido- and aqua-bridged heterometallic Fe(III)/Na(I) coordination polymer [Fe(N<sub>3</sub>)(μ-L)<sub>2</sub>(μ-O)<sub>1/2</sub>(Na)(μ-H<sub>2</sub>O)<sub>1/2</sub>]<sub>n</sub> (**4**) (Scheme 1).



Scheme 1. Synthesis of compounds 1–4.

In the FT-IR spectra of 1–4, the characteristic strong bands of the coordinated carboxylate groups appear at 1612–1652 cm<sup>-1</sup> or 1356–1368 cm<sup>-1</sup> for the asymmetric or the symmetric stretching, respectively. Asymmetrical and symmetrical N–H stretching frequencies of the amine groups appear in the 3442–3466 cm<sup>-1</sup> region. The bands at 1319–1339 cm<sup>-1</sup> are attributed to C–N stretch (aromatic amines) [37].

#### 3.2. Crystal Structure Analyses

According to the crystal structure analyses, complexes **1** and **2** are mononuclear and crystallize in different space groups (**1** in monoclinic C2/c and **2** in triclinic P-1). In **1**, the asymmetric unit contains three L<sup>-</sup> ligands coordinated to one Fe<sup>3+</sup> ion (Figure 1), whereas for **2**, the asymmetric unit contains two crystallographically independent metal complex cations—each one constructed from two L<sup>-</sup> and two chloride ligands coordinated to a Fe<sup>3+</sup> cation—and two non-coordinated triethylammonium counter-ions (Figure 2). In both cases, the iron(III) centers present octahedral-type geometries with N<sub>3</sub>O<sub>3</sub> (in **1**) and N<sub>2</sub>O<sub>2</sub>Cl<sub>2</sub> (in **2**) coordination environments, but the way the L<sup>-</sup> coordinates to the metal center depends on the structure. Thus, in **1**, the ligands are all the same, and the *trans*-O<sub>carboxylate</sub>/O<sub>carboxylate</sub>,

the *trans*-N<sub>pyrazine</sub>/N<sub>pyrazine</sub>, and the *trans*-O<sub>carboxylate</sub>/N<sub>pyrazine</sub> arrangements can be found. In the structure of **2**, the configurations around the metals in the two complex cations are different, and the *trans*-O<sub>carboxylate</sub>/N<sub>pyrazine</sub>, *trans*-N<sub>pyrazine</sub>/Cl, and *trans*-O<sub>carboxylate</sub>/Cl can be found at the Fe1 center and one *trans*-O<sub>carboxylate</sub>/O<sub>carboxylate</sub> and two *trans*-N<sub>pyrazine</sub>/Cl at the Fe2 one. The Fe-O bond lengths range from 1.882(12) to 2.047(3) Å, the Fe-N from 2.047(14) to 2.236(4) Å, and the Fe-Cl distance from 2.2691(16) to 2.2725(14) Å. Extensive H-bond interactions occur in both complexes. In **1**, the amine H-atoms intermolecularly connect with the non-coordinated O<sub>carboxylate</sub> generating a 2D zig-zag grid, but in **2**, a 1D chain type network is formed from alternating N<sub>amine</sub>H⋯O<sub>carboxylate</sub> and N<sub>amine</sub>H⋯N<sub>pyrazine</sub> contacts (Figure 2B). Moreover, in both complexes, we observe intramolecular resonance-assisted hydrogen bonding (RAHB) interactions between the N<sub>amine</sub>-H and the O<sub>carboxylate</sub> atoms, with the H⋯O<sub>carboxylate</sub> and N<sub>amine</sub>⋯O<sub>carboxylate</sub> distances in the ranges of 2.080 Å-2.145 Å and 2.701 Å-2.768 Å, respectively. The triethylammonium cations in **2** are hydrogen bonded to the complex cations through N-H⋯O [*d*<sub>D⋯A</sub> 2.844(6)-2.886(6) Å] and C-H⋯O [*d*<sub>D⋯A</sub> 3.179(16) Å] interactions. Furthermore, the chloro ligands also interact with the amine group [*d*<sub>D⋯A</sub> 3.445(5)-3.663(5) Å] and the aromatic carbons [*d*<sub>D⋯A</sub> 3.658(6) Å].

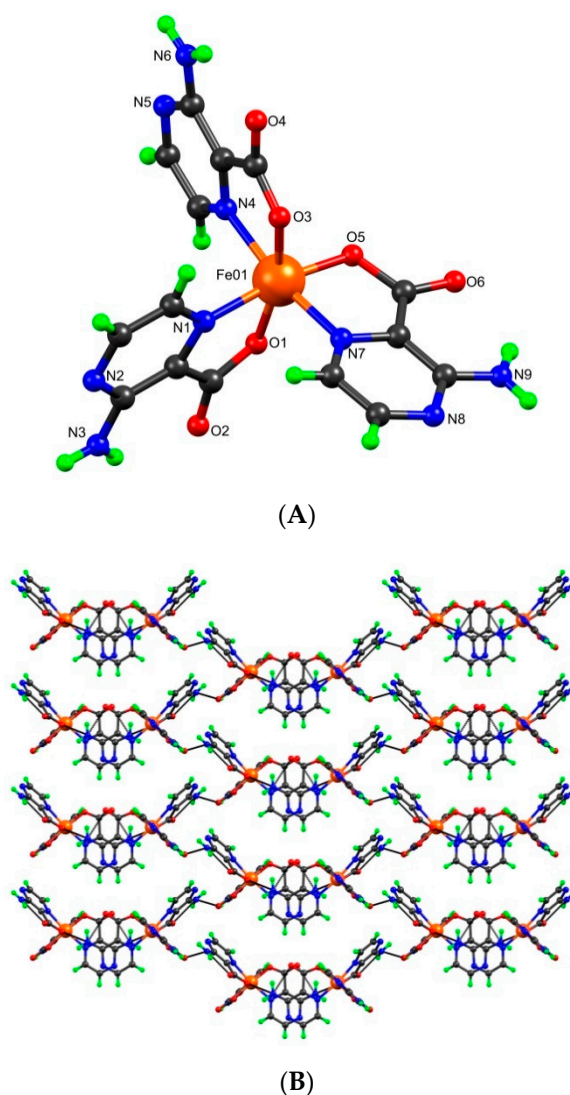


**Figure 1.** (A) Ball-and-stick representation of **1** with partial atom numbering scheme. (B) Its hydrogen-bonded 2D network.

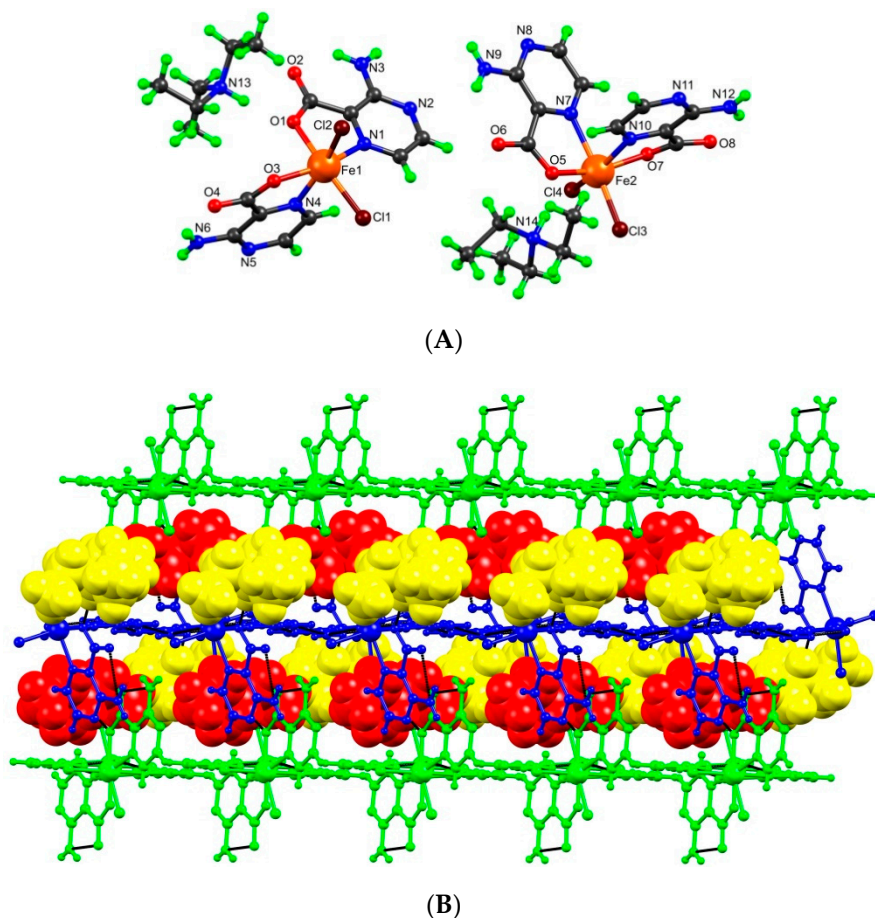


**Figure 2.** (A) Ball-and-stick representation of the two crystallographically independent complex units and counter-ions in **2** with partial atom numbering scheme. (B) Its hydrogen-bonded network (the NHEt<sub>3</sub><sup>+</sup> ions are represented in red and yellow space-fill model).

The crystal structure analysis revealed that **3** is a dimethoxido-bridged dinuclear Fe(III) complex, its asymmetric unit containing two L<sup>−</sup> ligands and one methoxido group coordinated to a Fe<sup>3+</sup> metal cation (Figure 3). The L<sup>−</sup> chelates the metal center through N<sub>pyrazine</sub> [Fe1-N1, 2.167(8) Å; Fe1-N4, 2.140(6) Å], O<sub>carboxylate</sub> [Fe1-O1, 1.972(6) Å; Fe1-O3, 1.991(5) Å], and the bridging methoxido is [Fe1-O5, 1.976(5) Å] therefore forming, upon symmetry expansion, a dinuclear structure. Thus, the conformations around the metals are equivalent: *trans*-O<sub>carboxylate</sub>/O<sub>carboxylate</sub> and *trans*-N<sub>pyrazine</sub>/O<sub>methoxo</sub>. The distance between the two symmetry-related Fe(III) centers is 3.035(2) Å and the Fe-O<sub>methoxo</sub>-Fe bond angle is around 100.4°. The hydrogen bond interactions in complex **3** involve the amine groups which donate to pyrazine N-atom, generating a one-dimensional chain spreading along the crystallographic *a* axis; further hydrogen contacts via N<sub>amine</sub>-H⋯O [*d*<sub>D⋯A</sub> 3.026(10) Å] lead to the formation of 2D extended network on the *ac* plane. Moreover, intramolecular resonance-assisted hydrogen bonding (RAHB) interactions between the amine and carboxylate groups [*d*<sub>D⋯A</sub> 2.719–2.758 Å] are also present in this complex.

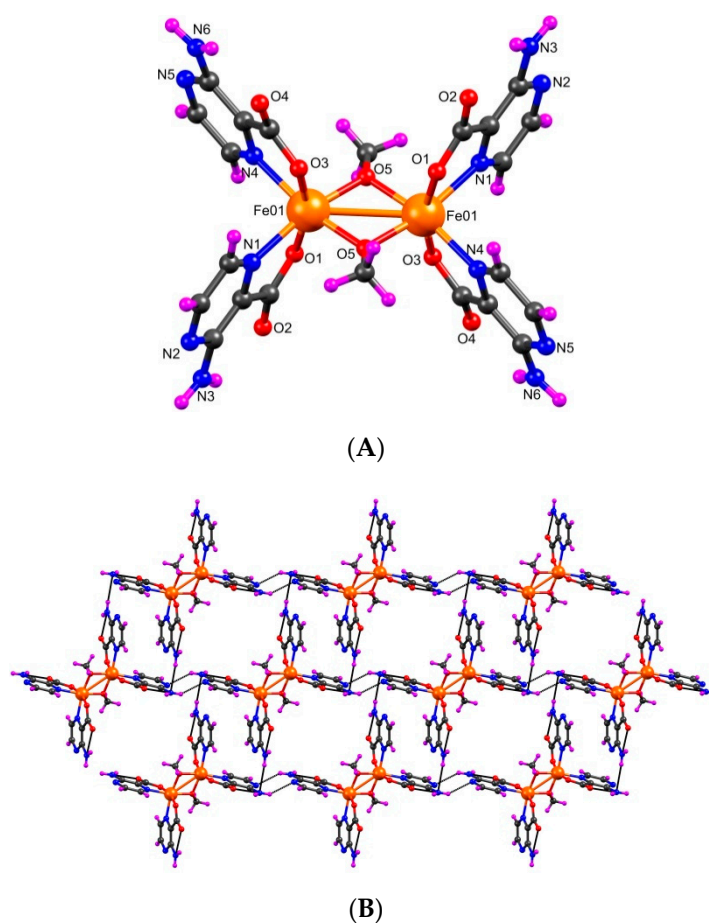


**Figure 3.** (A) Ball-and-stick representation of **3** with partial atom numbering scheme. (B) Its 2D hydrogen-bonded network.

The reaction of HL with  $\text{FeCl}_3$  and sodium azide in solvothermal condition leads to the formation of the 2D heterometallic network **4** (Figure 4C). Its asymmetric unit contains two  $\text{L}^-$  moieties, each one O- and  $\text{N}_{\text{pyrazine}}$ -bonded to a  $\text{Fe}^{3+}$  cation, its octahedral type coordination sphere being completed with an  $\text{N}_{\text{azide}}$  and half an  $\text{O}_{\text{oxo}}$  anion; a  $\text{Na}^+$  cation linked to the  $\text{N}_{\text{pyrazine}}$  of one of the  $\text{L}^-$  groups and a coordinated water molecule were also found (Figure 4A). Symmetry expansion reveals a hexa-coordination sodium center with the carboxylate groups of two  $\text{L}^-$  acting in a chelating mode (Figure 4B). In this way, the 2D polymer is formed by sheets of iron and sodium cations connected by the organic moieties, the oxido anions, and the water molecules, respectively, bridging the Fe(III) and the Na(I) centers, thus connecting two infinite sheets. The Fe–O bond length of the  $\mu$ -oxido diiron(III) core is approximately 1.772 Å, the Fe– $\text{O}_{\text{oxo}}$ –Fe bond angle is approximately  $180^\circ$ , and the distance between the two symmetry-related Fe(III) centers is 3.544 Å; these values are in the range of those observed for other iron(III)  $\mu$ -oxido-bridged complexes [38]. The distance between the two symmetry-related Na(I) centers is 3.963 Å, and the Na– $\text{O}_{\text{water}}$ –Na bond angle is  $113.3^\circ$ . This is the first example of an oxido- and aqua-bridged heterometallic Fe(III)–Na(I) coordination polymer based on the 3-amino-2-pyrazinecarboxylic acid proligand. The oxido-bridged diiron(III) core has structural resemblance with one of the intermediate structures of methane monooxygenase during the catalytic conversion of methane to methanol [38]. Extensive H-bond interactions can be found that play a role towards the extension to 3D supramolecular frameworks. A list of selected hydrogen bonding interactions is presented in Table S3 (Supplementary Materials). In this framework, intramolecular resonance-assisted N–H $\cdots$ O hydrogen bonding as well as various C–H $\cdots$ O interactions play a significant role in stabilizing the structure and extending it to the third dimension.

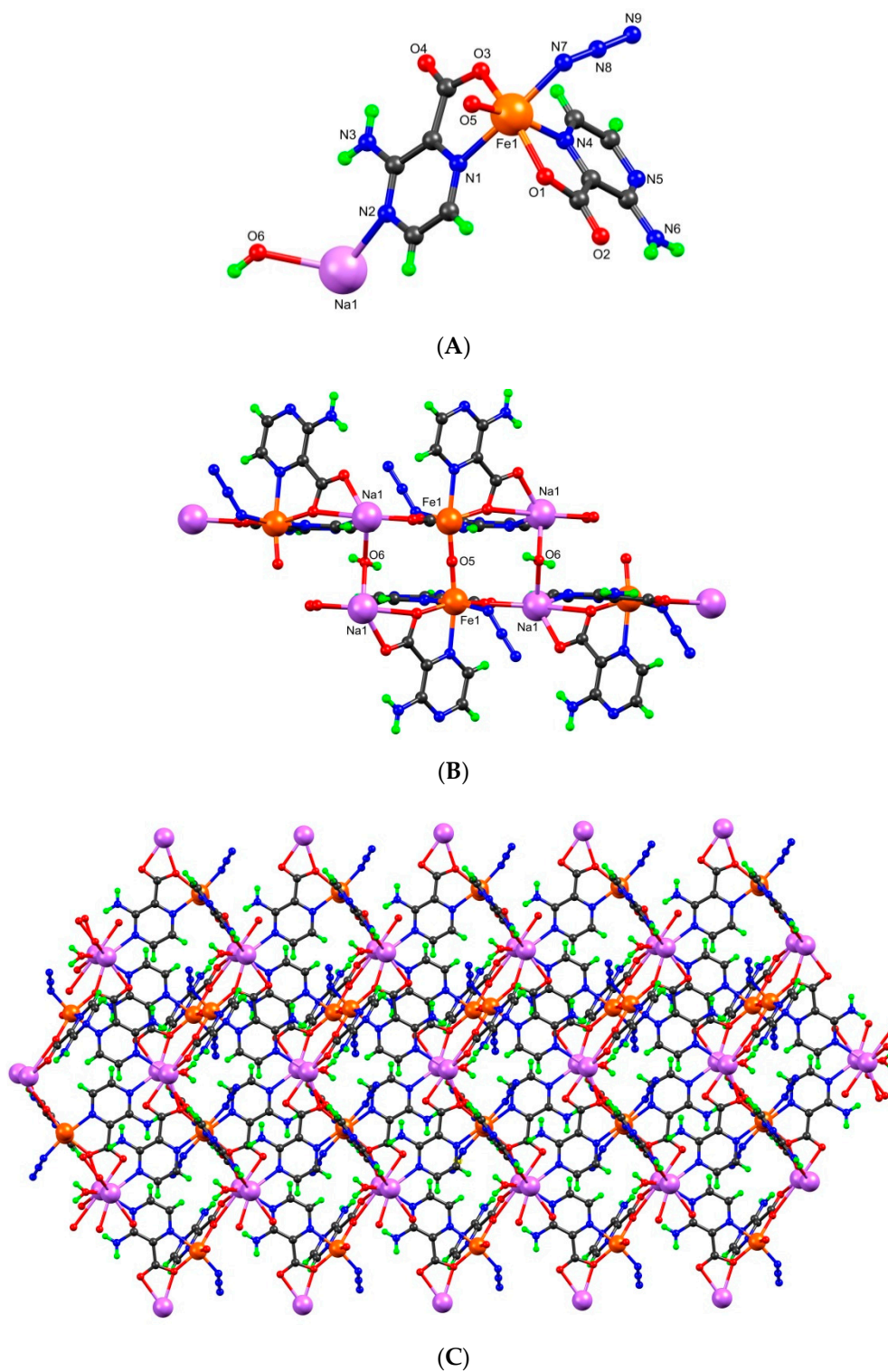
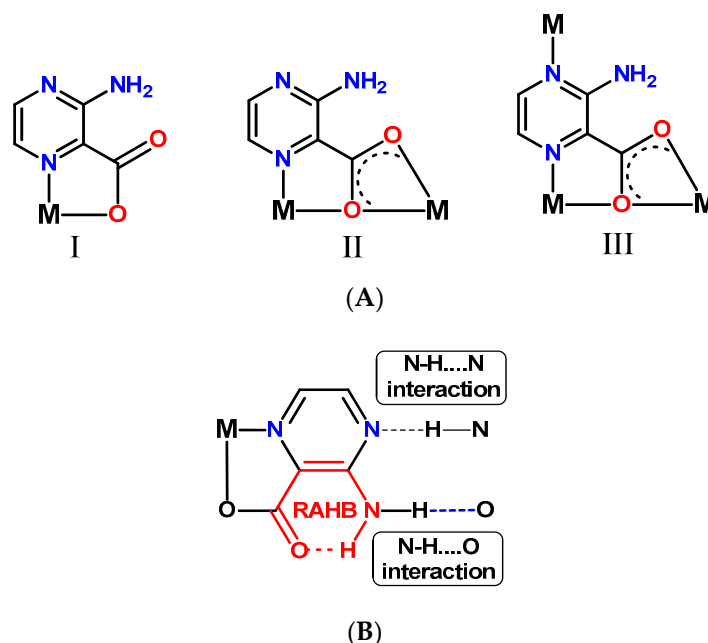


**Figure 4.** (A) Ball-and-stick representation of the asymmetric unit of coordination polymer 4 with partial atom numbering scheme, (B) its crystal structure, and (C) two-dimensional depiction (arbitrary view).

The 3-amino-2-pyrazinecarboxylate ligand in the compounds of this study exhibits three different coordination modes, shown in Scheme 2A. Mode I is the most common and is present in complexes 1, 2, and 3;  $L^-$  acts as a N,O-bidentate chelating ligand and coordinates to one Fe(III) center. Modes II and III are only found in the coordination polymer 4; the carboxylate group itself acts as a bridging chelate ligand, and in III, the pyrazine-N is also involved in coordination. Additionally, the 3-amino-2-pyrazinecarboxylate ligand is involved in various hydrogen bond interactions such as N-H...O, N-H...N, or intramolecular resonance-assisted hydrogen bonding (RAHB) contacts (Scheme 2B).



**Scheme 2.** Coordination (A) and hydrogen bonding (B) modes of the  $L^-$  ligand in compounds 1–4.

### 3.3. Hirshfeld Surface Analysis

Hirshfeld surface analysis provides an effective tool to analyze the differences in crystal packing between structurally related compounds. It is a useful for visualizing 3-dimensional electron density, especially that related to intermolecular interactions. We used the Crystal Explorer program [39] for this task. Hirshfeld surface plots and 2D fingerprints of intermolecular interactions for compounds 1–4 are presented in Figure 5. In all compounds, we observe four significant contacts, i.e.,  $O\cdots H$  (16.6–35.2%),  $N\cdots H$  (11.3–26.3%),  $H\cdots H$  (12.6–39.3%), and  $C\cdots H$  (6.4–12.4%). In addition, a  $Cl\cdots H$  (25.7%) interaction also occurs in 2 (Figure S1, Supplementary Materials). For compound 1, the most significant contributions come from  $H\cdots O$  (35.2%) contacts, which correspond to the  $N-H\cdots O/C-H\cdots O$  interactions. However, for compounds 2 and 3, a higher contribution comes from  $Cl\cdots H$  (25.7%) and  $H\cdots H$  (39.3%) contacts, respectively. However, for 4, the predominant interaction is  $N\cdots H$  (26.3%). In these compounds,  $C\cdots C$  (1.2–3.3%) contacts occur to a lower extent, which significantly proves that they do not have relevant  $\pi$ - $\pi$  interactions.

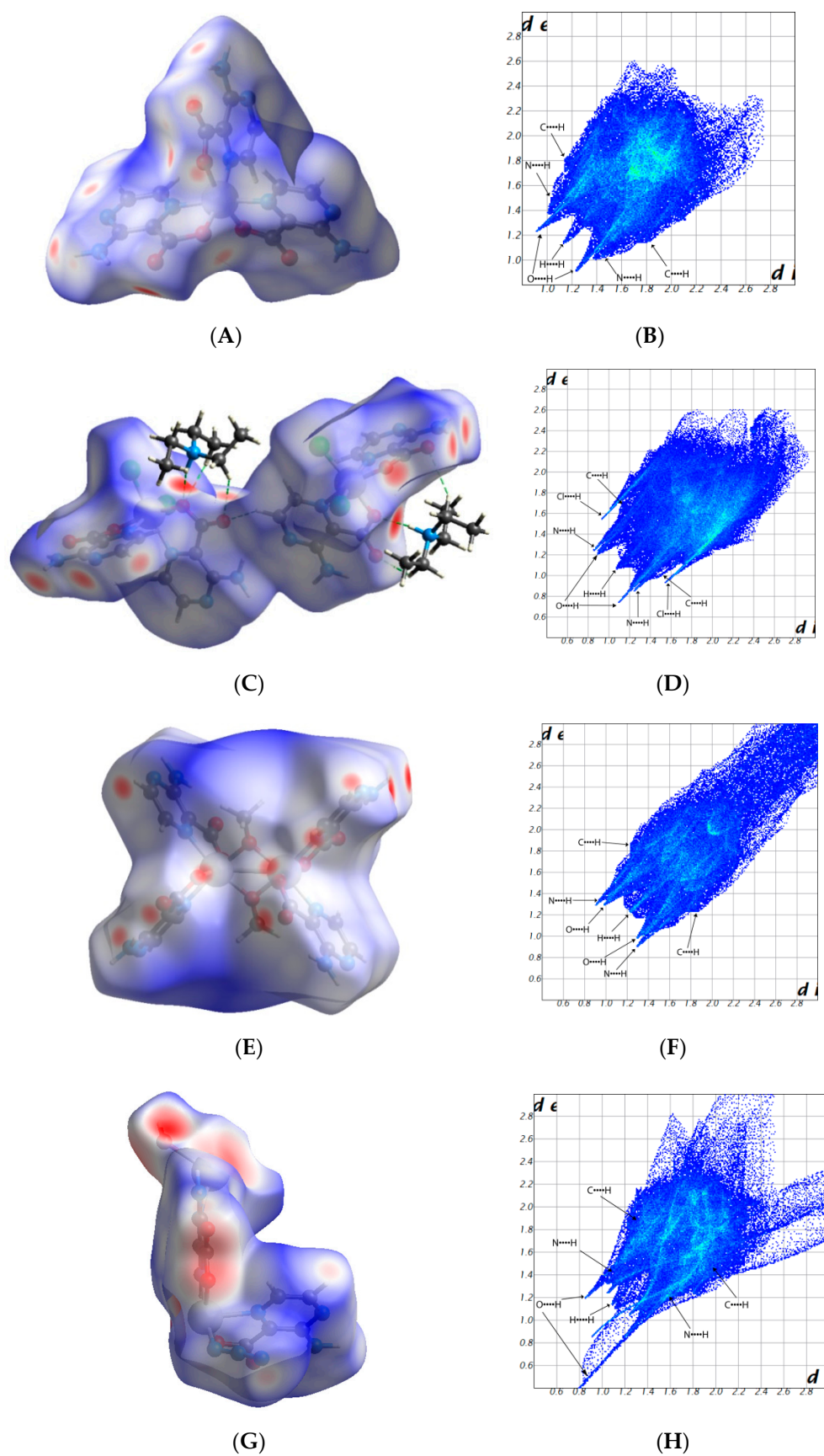
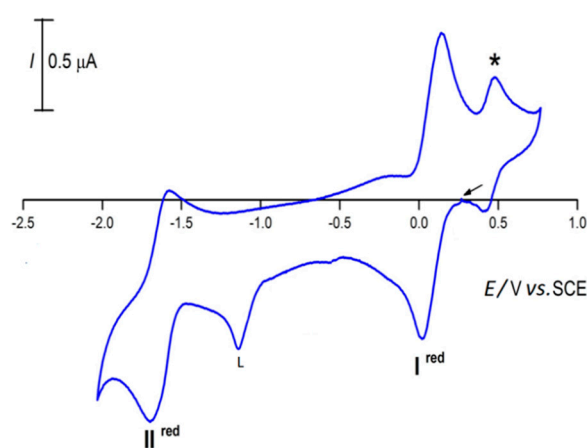


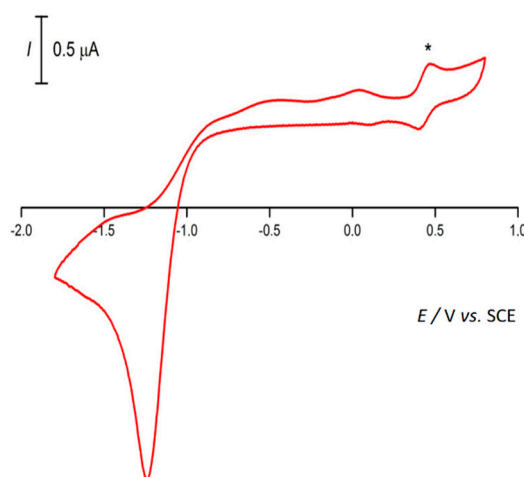
**Figure 5.** Calculated Hirshfeld surfaces of compounds 1 (A), 2 (C), 3 (E), and 4 (G). The red spots on the Hirshfeld maps correspond to close intermolecular interactions, whereas blue regions are the domains without close intermolecular contacts. 2D fingerprint plots of 1 (B), 2 (D), 3 (F), and 4 (H) exhibit different intermolecular interactions.

### 3.4. Electrochemistry of Compounds 1–4

At a platinum electrode, at 25 °C in 0.2 M  $[\text{NBu}_4][\text{BF}_4]/\text{DMSO}$  solution and in the  $0.05\text{--}1.0\text{ V s}^{-1}$  range of scan rates, complexes 1–4 show similar cyclic voltammograms (such a typical cyclic voltammetric behavior is illustrated for **4** in Figure 6A; for all the compounds, see Figure S3 in the Supplementary Materials). They exhibit one reversible single-electron reduction (wave I) at a half-wave potential value  $^{\text{I}}E_{1/2}^{\text{red}}$  of approximately 0.08 V vs. SCE (Table 1), assigned to  $\text{Fe(III)} \rightarrow \text{Fe(II)}$  reduction, and a second one (wave II) also reversible at a half-wave potential value  $^{\text{II}}E_{1/2}^{\text{red}}$  of approximately  $-1.65\text{ V}$  vs. SCE (Table 1), assigned to  $\text{Fe(II)} \rightarrow \text{Fe(I)}$  reduction. The number of electrons involved in each wave was confirmed by controlled potential electrolysis (CPE; see experimental). The first reduction potential of complexes 1–4 possibly is an important factor for their catalytic performance in the peroxidative oxidation of cyclohexanol to cyclohexanone, as the availability of easily reducible iron(III) species by the TBHP is crucial for the oxidation process to initiate (see below, Equation (1)).



(A)



(B)

**Figure 6.** Cyclic voltammogram, initiated by the cathodic sweep, of (A) **4** or (B) HL in a 0.2 M  $[\text{NBu}_4\text{N}][\text{BF}_4]/\text{DMSO}$  solution, at a Pt disc working electrode ( $d = 0.5\text{ mm}$ ), run at a scan rate of  $100\text{ mVs}^{-1}$ . \*  $[\text{Fe}(\eta^5\text{-C}_5\text{H}_5)_2]^{0/+}$ .

**Table 1.** Cyclic voltammetric data<sup>a</sup> for the Fe(III) complexes 1–4.

Complex	I $E_{\frac{1}{2}}$ red	II $E_{\frac{1}{2}}$ red
1	0.079	−1.638
2	0.076	−1.646
3	0.074	−1.654
4	0.076	−1.655

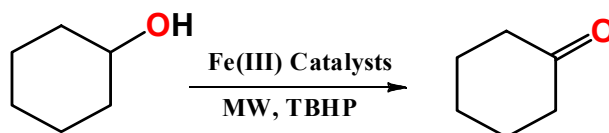
<sup>a</sup> Values in V vs. SCE, in a 0.2 M [Bu<sub>4</sub>N][BF<sub>4</sub>]/DMSO solution, at a Pt disc working electrode, determined by using the [Fe( $\eta^5$ -C<sub>5</sub>H<sub>5</sub>)<sub>2</sub>]<sup>0/+</sup> redox couple ( $E_{1/2}^{ox}$  = 0.42 V vs. SCE) [32] as internal standard at a scan rate of 100 mVs<sup>−1</sup>.

A reduction centered at the 3-amino-2-pyrazinecarboxylate ligand is also detected in the above voltammograms (irreversible reduction wave at −1.04 V vs. SCE, a value close to that of the reduction exhibited by HL under identical experimental conditions—Figure 6B).

However, we should be cautious with the assignment of the peaks, since the high similarities of the CVs and of the mass spectra (ESI-MS) of the [NBu<sub>4</sub>][BF<sub>4</sub>]/DMSO solutions of all the compounds suggest that in this medium they convert into common species. The observed common peak at  $m/z$  570 in the ESI-MS (positive mode) spectra can tentatively be assigned to Na[Fe(L)<sub>3</sub>(DMSO)]<sup>+</sup>.

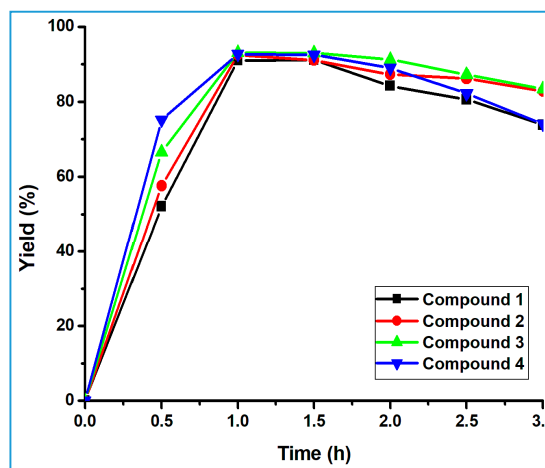
#### 4. Microwave-Assisted Catalytic Peroxidative Oxidation of Cyclohexanol to Cyclohexanone

The oxidation of cyclohexanol to cyclohexanone was chosen as a model alcohol oxidation reaction, aiming to improve its sustainability. In fact, an industrially important step of the polycaprolactam production process involves the non-sustainable oxidation of KA oil (cyclohexanol and cyclohexanone mixture) to pure cyclohexanone catalyzed by Cu and Cr oxides at 250 °C and high pressure [27]. Thus, complexes 1–4 were tested as catalysts for the microwave (MW)-assisted oxidation of cyclohexanol using aqueous *tert*-butyl hydroperoxide (*t*BuOOH or TBHP, aq. 70%) as the oxidizing agent at 60–80 °C under low power (10–50 W) MW irradiation (0.5–3 h reaction time) and in the absence of any added solvent and in additive-free medium (Scheme 3).

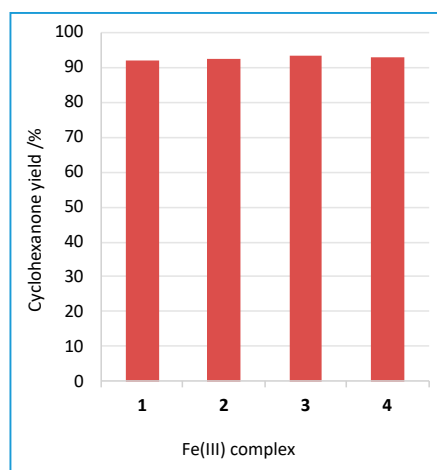
**Scheme 3.** MW-assisted oxidation of cyclohexanol to cyclohexanone catalyzed by 1–4.

Under the optimized conditions (Table S4), 1 h of irradiation (10 W) at 70 °C, 91.0%–93.1% yield of cyclohexanone was obtained from the MW-assisted oxidation of cyclohexanol in the presence of 0.1 mol% vs. substrate of 1–4 (TOFs up to  $1.50 \times 10^3$  h<sup>−1</sup>, entry 62, Table S4) with a selectivity of 100%. Indeed, no traces of by-products were detected by GC-MS analysis in the final reaction mixtures for the above conditions. Moreover, control experiments in the absence of the Fe(III) complex led only to 7% of alcohol conversion, highlighting the crucial role of 1–4 to efficiently catalyze the oxidation of cyclohexanol.

The very similar catalytic activities of 1–4 (Figure 7) are in accord with their very similar reduction potentials as detected by cyclic voltammetry (see above), which conceivably determine the iron-promoted decomposition of TBHP (see mechanistic considerations below).



(A)

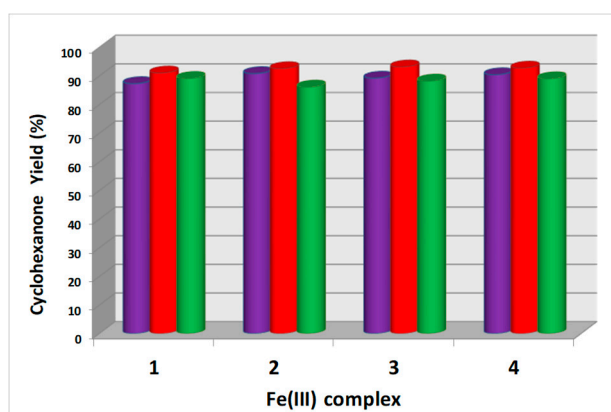


(B)

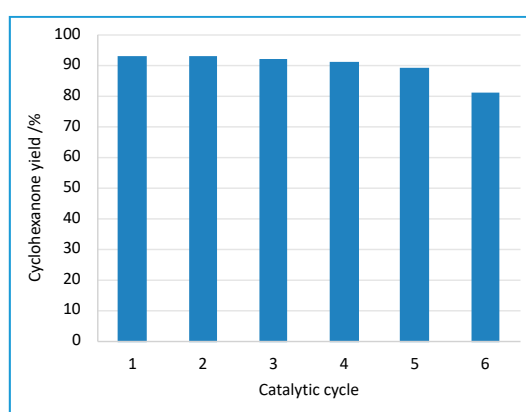
**Figure 7.** (A) Plots of yield vs. time for the microwave (MW)-assisted oxidation of cyclohexanol by *tert*-butylhydroperoxide catalyzed by frameworks 1–4. (B) Maximum yield of cyclohexanone obtained from the same reaction.

It is worth mentioning that such a high conversion of cyclohexanol into cyclohexanone is scarcely reported [40–42], and the present catalysts 1–4 are among the most active and selective ones for this industrially important reaction. For example, Fe(III) complexes derived from *N*-acetylpyrazine-2-carbohydrazide, viz., the mononuclear  $[\text{Fe}(\text{kNN}'\text{O-HL})\text{Cl}_2]$  and the binuclear  $[\text{Fe}(\text{kNN}'\text{O-HL})\text{Cl}(\mu\text{-OMe})_2]$ , when used as catalysts for the oxidation of cyclohexanol with TBHP under solvent-free MW irradiation conditions, led to yields up to 36% and 37%, respectively, of cyclohexanone after 1 h at 120 °C [42]. Moreover, decomposition at the reaction media impaired their reuse in further catalytic cycles. Therefore, this study may be of significance towards the improvement of the sustainability of polycaprolactam manufacture.

A very favorable effect of MW irradiation is observed in this study even at the applied low power of 10 W. For example, for 3, the cyclohexanone yield increases from 18% (obtained using an oil bath heating) to 93.1% upon MW irradiation, the other conditions being the same. An increase of the reaction temperature from 60 °C to 70 °C enhanced the product yield from 89.2% to 93.1% after 1 h of reaction time, for compound 3 as catalyst (entries 38 and 44, Table S4), whereas a further raise in temperature to 80 °C resulted in a decrease in reaction yield to 88.2% (entry 51, Table S4, Figure 8A). We have also observed a similar phenomenon for the other compounds (1, 2, and 4) (Figure 8A).



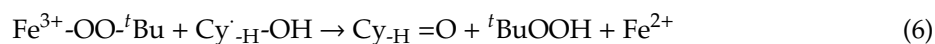
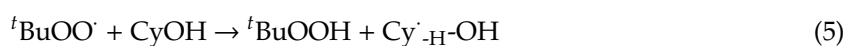
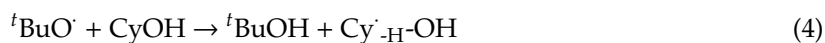
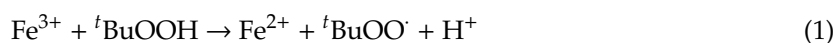
(A)



(B)

**Figure 8.** (A) Influence of the temperature on the yield of cyclohexanone obtained by MW-assisted oxidation of cyclohexanol with *tert*-butyl hydroperoxide (TBHP) after 1 h reaction time (purple pillars = reactions performed at 60 °C; red pillars = reactions performed at 70 °C, and green pillars = reactions performed at 80 °C). (B) Maximum yield of cyclohexanone obtained in consecutive recycles of the MW-assisted oxidation of cyclohexanol by *tert*-butylhydroperoxide catalyzed by **3** after 1 h reaction time.

Evidence for a free-radical mechanism, as previously proposed [28], arises from addition of the  $\text{CBrCl}_3$  or  $\text{Ph}_2\text{NH}$  radical trap to the reaction mixture, that results in the almost suppression of the catalytic activity compared to the reaction carried out under the same conditions (5 mmol, 70 °C, MW, 1 h) but in the absence of a radical trap. This suggests the generation of oxygen and carbon radicals in the reaction, which are trapped by such radical scavengers. Thus, the mechanism of cyclohexanol oxidation (see Equations (1)–(6)) may involve the  ${}^t\text{BuO}^\cdot$  and  ${}^t\text{BuOO}^\cdot$  radicals produced in the iron promoted decomposition of TBHP [23] according to Equations (1)–(6), where Cy denotes cyclohexyl and  $\text{Cy}^\cdot\text{-H-OH}$  denotes the radical formed upon H-abstraction from cyclohexanol  $\text{CyOH}$  [43–46].



The catalysts of the present study, being heterogeneous, present the additional advantage of being recyclable. Recycling of catalyst 3 was tested up to six consecutive cycles, and it was found that it maintains almost at the original level of activity for five cycles. After the sixth cycle, 3 retains 87% of its initial activity (Figure 8B). The FT-IR spectra of catalyst 3 were taken before and after the catalysis and no significant change was observed, what suggests that the structure of the solid was retained (Figure S2, Supplementary Materials). Moreover, the amount of iron determined in the filtrate solution, obtained after the separation of the catalyst 3, was only 0.010% of the amount used in the reaction, thus ruling out any significant leaching of the catalyst.

## 5. Concluding Remarks

Four novel iron(III) coordination compounds were derived from 3-amino-2-pyrazinecarboxylic acid (HL) under various synthetic conditions. They exhibit mononuclear (1 and 2), dinuclear (3), and 2D heterometallic polymeric (4) structures, on account of the various coordination modes of  $L^-$ . Single-crystal X-ray diffraction analysis revealed that 1 and 2 have different mononuclear structures, the latter with two different and crystallographically independent complex metal cations, whereas compound 3 has a methoxido-bridged dinuclear structure. Compound 4 features the first example of a two dimensional oxido- and aqua-bridged heterometallic Na(I)/Fe(III) polynuclear coordination polymer based on such a ligand. In all compounds, the Fe(III) centers adopted octahedral type coordination environments.

Cyclic voltammetric studies, supported by controlled potential electrolyses, indicate that complexes 1–4 easily undergo reversible Fe(III) to Fe(II) reductions at a positive potential (0.08 V) vs. SCE, thus being easily reduceable (good oxidants), which is in line with their ability to act as efficient heterogeneous catalysts for the mild additive-free microwave-assisted peroxidative oxidation of cyclohexanol to cyclohexanone. Thus, the electrochemical studies appear as a useful tool to assign the ability of a metal complex to behave as an oxidant and, therefore, to predict its catalytic performance in oxidation catalysis. Moreover, the catalysts were easily recovered and reused, at least for five consecutive cycles, maintaining a high selectivity and activity.

**Supplementary Materials:** The following are available online at <http://www.mdpi.com/2076-3417/10/8/2692/s1>, Figure S1: 2D fingerprint plots of 1–4, exhibiting different intermolecular interactions, Figure S2: FT-IR spectra of 3 before (in blue), after (in red) the microwave-assisted catalytic peroxidative oxidation of cyclohexanol, Figure S3: Cyclic voltammograms (current intensity in  $\mu A$  vs. potential in V), initiated by the anodic sweep, of compounds 1–4 in a 0.2 M [ $n$ Bu<sub>4</sub>N][BF<sub>4</sub>]/DMSO solution, at a Pt disc working electrode. Internal standard used: [Fe( $\eta^5$ -C<sub>5</sub>H<sub>5</sub>)<sub>2</sub>]<sup>0/+</sup> redox couple ( $E_{1/2}^{ox} = 0.42$  V vs. SCE), Table S1: Crystal data and structure refinement details for compounds 1–4, Table S2: Selected bond distances (Å) and angles (°) for compounds 1–4, Table S3: Hydrogen bond geometry (Å, °) in compounds 1–4, Table S4: MW-assisted oxidation of cyclohexanol to cyclohexanone with TBHP and catalyzed by 1–4.

**Author Contributions:** A.K.: Research planning, synthesis and characterization of complexes, Hirshfeld Surface Analysis, manuscript writing. L.M.D.R.S.M.: Catalytic studies. Y.Y.: Electrochemistry and Catalytic studies. M.F.C.G.d.S.: Single crystal X-ray diffraction analysis of compounds. A.J.L.P.: Manuscript reading and correcting. All authors have read and agreed to the published version of the manuscript.

**Funding:** This research was funded by [Fundação para a Ciência e Tecnologia (FCT)] grant number [UIDB/00100/2020].

**Acknowledgments:** A. Karmakar expresses his gratitude to the FCT and Instituto Superior Técnico for Scientific Employment contract (Contrato No: IST-ID/107/2018) under Decree-Law no. 57/2016, of August 29.

**Conflicts of Interest:** There is no conflict of interest.

## References

1. Vernik, I.; Stynes, D.V. ( $\mu$ -Oxo)diiron Complexes of Gated Glyoximes. Structural Changes Accompanying Ligation Trans to the Oxo Bridge. *Inorg. Chem.* **1996**, *35*, 2006–2010. [[CrossRef](#)]
2. Feig, A.L.; Lippard, S.J. Reactions of Non-Heme Iron(II) Centers with Dioxygen in Biology and Chemistry. *Chem. Rev.* **1994**, *94*, 759–805. [[CrossRef](#)]

3. True, A.E.; Scarrow, R.C.; Randall, C.R.; Holz, R.C.; Que, L. EXAFS studies of uteroferrin and its anion complexes. *J. Am. Chem. Soc.* **1993**, *115*, 4246–4255. [[CrossRef](#)]
4. Nordlund, P.; Eklund, H. Structure and function of the Escherichia coli ribonucleotide reductase protein R2. *J. Mol. Biol.* **1993**, *232*, 123–164. [[CrossRef](#)] [[PubMed](#)]
5. Solomon, E.I.; Brunold, T.C.; Davis, M.I.; Kemsley, J.N.; Lee, S.-K.; Lehnert, N.; Neese, F.; Skulan, A.J.; Yang, Y.-S.; Zhou, J. Geometric and Electronic Structure/Function Correlations in Non-Heme Iron Enzymes. *Chem. Rev.* **2000**, *100*, 235–350. [[CrossRef](#)] [[PubMed](#)]
6. Parrilha, G.L.; Fernandes, C.; Bortoluzzi, A.J.; Szpoganicz, B.; Silva, M.S.; Pich, C.T.; Terenzi, H.; Horn, A., Jr. A new  $\mu$ -oxo di-iron complex with suitable features to mimic metallohydrolase activity: X-ray molecular structure, aqua solution behavior and nuclease activity of the complex  $[\text{Fe}(\text{HPCINOL})(\text{SO}_4)]_2\text{-}\mu\text{-oxo}$ . *Inorg. Chem. Commun.* **2008**, *11*, 643–647. [[CrossRef](#)]
7. Biswas, R.; Drew, M.G.B.; Estarellas, C.; Frontera, A.; Ghosh, A. Synthesis and Crystal Structures of  $\mu$ -Oxido- and  $\mu$ -Hydroxido-Bridged Dinuclear Iron(III) Complexes with an  $\text{N}_2\text{O}$  Donor Ligand—A Theoretical Study on the Influence of Weak Forces on the Fe–O–Fe Bridging Angle. *Eur. J. Inorg. Chem.* **2011**, *2011*, 2558–2566. [[CrossRef](#)]
8. Naiya, S.; Drew, M.G.B.; Diaz, C.; Ribas, J.; Ghosh, A. Synthesis, Crystal Structure, and Magnetic Properties of a Very Rare Double  $\mu$ -1,1-Azido- and a  $\mu$ -1,1-(OMe)-Bridged Fe(III) Dimer Containing a N,N,O-Donor Tridentate Schiff Base Ligand. *Eur. J. Inorg. Chem.* **2011**, *2011*, 4993–4999. [[CrossRef](#)]
9. Negoro, S.; Asada, H.; Fujiwara, M.; Matsushita, T. Preparation and characterization of three types of dinuclear iron(III) complexes with  $\text{H}_2\text{salbn}$ , N,N'-disalicylidene-1,4-diaminobutane. *Inorg. Chem. Commun.* **2003**, *6*, 357–360. [[CrossRef](#)]
10. Hazra, S.; Bhattacharya, S.; Singh, M.K.; Carrella, L.; Rentschler, E.; Weyhermueller, T.; Rajaraman, G.; Mohanta, S. Syntheses, Structures, Magnetic Properties, and Density Functional Theory Magneto-Structural Correlations of Bis( $\mu$ -phenoxo) and Bis( $\mu$ -phenoxo)- $\mu$ -acetate/Bis( $\mu$ -phenoxo)-bis( $\mu$ -acetate) Dinuclear Fe(III)Ni(II) Compounds. *Inorg. Chem.* **2013**, *52*, 12881–12892. [[CrossRef](#)]
11. Berto, T.C.; Speelman, A.L.; Zheng, S.; Lehnert, N. Mono- and dinuclear non-heme iron–nitrosyl complexes: Models for key intermediates in bacterial nitric oxide reductases. *Coord. Chem. Rev.* **2013**, *257*, 244–259. [[CrossRef](#)]
12. Hill, R.J.; Long, D.L.; Champness, N.R.; Hubberstey, P.; Schroder, M. New Approaches to the Analysis of High Connectivity Materials: Design Frameworks Based upon 44- and 63-Subnet Tectons. *Acc. Chem. Res.* **2005**, *38*, 335–348. [[CrossRef](#)] [[PubMed](#)]
13. Tanase, S.; Marques Gallego, P.; Bouwman, E.; Long, G.J.; Rebbouh, L.; Grandjean, F.; de Gelder, R.; Mutikainen, I.; Turpeinen, U.; Reedijk, J. Versatility in the binding of 2-pyrazinecarboxylate with iron. Synthesis, structure and magnetic properties of iron(ii) and iron(iii) complexes. *Dalton Trans.* **2006**, *13*, 1675–1684. [[CrossRef](#)]
14. Starosta, W.; Leciejewicz, J. catena-Poly[[bis( $\mu$ -3-aminopyrazine-2-carboxylato)- $\kappa^3\text{N}^1, \text{O}:\text{O}$ ;  $\kappa^3\text{O}:\text{N}^1, \text{O}$ ]-dilithium]-di- $\mu$ -aqua]. *Acta Cryst.* **2010**, *66*, m744–m745. [[CrossRef](#)] [[PubMed](#)]
15. Gao, S.; Ng, S.W. (3-Aminopyrazin-4-ium-2-carboxylate- $\kappa^2\text{N}^1, \text{O}$ ) diaquazinc(II) dinitrate. *Acta Cryst.* **2010**, *66*, m1466. [[CrossRef](#)]
16. Deng, Z.-P.; Kang, W.; Huo, L.-H.; Zhao, H.; Gao, S. Rare-earth organic frameworks involving three types of architecture tuned by the lanthanide contraction effect: Hydrothermal syntheses, structures and luminescence. *Dalton Trans.* **2010**, *39*, 6276–6284. [[CrossRef](#)]
17. Karmakar, A.; Hazra, S.; Rúbio, G.M.D.M.; da Guedes Silva, M.F.C.; Pombeiro, A.J.L. Packing polymorphism in 3-amino-2-pyrazinecarboxylate based tin(ii) complexes and their catalytic activity towards cyanosilylation of aldehydes. *New J. Chem.* **2018**, *42*, 17513–17523. [[CrossRef](#)]
18. Karmakar, A.; Martins, L.M.D.R.S.; da Guedes Silva, M.F.C.; Hazra, S.; Pombeiro, A.J.L. Solvent-Free Microwave-Assisted Peroxidative Oxidation of Alcohols Catalyzed by Iron(III)-TEMPO Catalytic Systems. *Catal. Lett.* **2015**, *145*, 2066–2076. [[CrossRef](#)]
19. Karmakar, A.; Hazra, S.; da Guedes Silva, M.F.C.; Pombeiro, A.J.L. Synthesis, structure and catalytic application of lead(ii) complexes in cyanosilylation reactions. *Dalton Trans.* **2015**, *44*, 268–280. [[CrossRef](#)]
20. Boudalis, A.K.; Sanakis, Y.; Dahan, F.; Hendrich, M.; Tuchagues, J.-P. An Octanuclear Complex Containing the  $[\text{Fe}_3\text{O}]^{7+}$  Metal Core: Structural, Magnetic, Mössbauer, and Electron Paramagnetic Resonance Studies. *Inorg. Chem.* **2006**, *45*, 443–453. [[CrossRef](#)]

21. Phillips, A.M.F.; Pombeiro, A.J.L.; Kopylovich, M.N. Recent Advances in Cascade Reactions Initiated by Alcohol Oxidation. *ChemCatChem* **2017**, *9*, 217–246. [[CrossRef](#)]
22. Gryca, I.; Machura, B.; Małecki, J.G.; Shul'pina, L.S.; Pombeiro, A.J.L.; Shul'pin, G.B. New p-tolylimido rhenium(V) complexes with carboxylate-based ligands: Synthesis, structures and their catalytic potential in oxidations with peroxides. *Dalton Trans.* **2014**, *43*, 5759–5776. [[CrossRef](#)] [[PubMed](#)]
23. Kopylovich, M.N.; Ribeiro, A.P.C.; Alegria, E.C.B.A.; Martins, N.M.R.; Martins, L.M.D.R.S.; Pombeiro, A.J.L. Catalytic Oxidation of Alcohols: Recent Advances. *Adv. Organomet. Chem.* **2015**, *63*, 91–174.
24. Schröder, K.; Join, B.; Amali, A.J.; Junge, K.; Ribas, X.; Costas, M.; Beller, M. A Biomimetic Iron Catalyst for the Epoxidation of Olefins with Molecular Oxygen at Room Temperature. *Angew. Chem. Int. Ed.* **2011**, *6*, 1425–1429. [[CrossRef](#)]
25. Kinen, C.O.; Rossi, L.I.; de Rossi, R.H. Mechanism of the Selective Sulfide Oxidation Promoted by HNO<sub>3</sub>/FeBr<sub>3</sub>. *J. Org. Chem.* **2009**, *74*, 7132–7139. [[CrossRef](#)] [[PubMed](#)]
26. Chen, M.; White, M.C. Combined Effects on Selectivity in Fe-Catalyzed Methylene Oxidation. *Science* **2010**, *327*, 566–571. [[CrossRef](#)]
27. Ribeiro, A.P.C.; Martins, L.M.D.R.S.; Carabineiro, S.A.C.; Buijnsters, J.G.; Figueiredo, J.L.; Pombeiro, A.J.L. Heterogenized C-Scorpionate Iron(II) Complex on Nanostructured Carbon Materials as Recyclable Catalysts for Microwave-Assisted Oxidation Reactions. *ChemCatChem* **2018**, *10*, 1821. [[CrossRef](#)]
28. Martins, M.D.R.S.; Ribeiro, A.P.C.; Carabineiro, S.A.C.; Figueiredo, J.L.; Pombeiro, A.J.L. Highly efficient and reusable CNT supported iron(ii) catalyst for microwave assisted alcohol oxidation. *Dalton Trans.* **2016**, *45*, 6816–6819. [[CrossRef](#)]
29. Ribeiro, A.P.C.; Martins, L.M.D.R.S.; Kuznetsov, M.L.; Pombeiro, A.J.L. Tuning Cyclohexane Oxidation: Combination of Microwave Irradiation and Ionic Liquid with the C-Scorpionate [FeCl<sub>2</sub>(Tpm)] Catalyst. *Organometallics* **2017**, *36*, 192–198. [[CrossRef](#)]
30. Nizova, G.V.; Krebs, B.; Süß-Fink, G.; Schindler, S.; Westerheide, L.; Cuervo, L.G.; Shul'pin, G.B. Hydroperoxidation of methane and other alkanes with H<sub>2</sub>O<sub>2</sub> catalyzed by a dinuclear iron complex and an amino acid. *Tetrahedron* **2002**, *58*, 9231–9237. [[CrossRef](#)]
31. Ellis, W.B. *Ullmann's Encyclopedia of Industrial Chemistry*, 6th ed.; Chiusoli, G.P., Maitlis, P.M., Eds.; Wiley-VCH: Weinheim, Germany, 1999; pp. 192–195.
32. Reisner, E.; Arion, V.B.; da Guedes Silva, M.F.C.; Lichtenecker, R.; Eichinger, A.; Keppler, B.K.; Yu Kukushkin, V.; Pombeiro, A.J.L. Tuning of Redox Potentials for the Design of Ruthenium Anticancer Drugs—An Electrochemical Study of [trans-RuCl<sub>4</sub>L(DMSO)]<sup>−</sup> and [trans-RuCl<sub>4</sub>L<sub>2</sub>]<sup>−</sup> Complexes, where L = Imidazole, 1,2,4-Triazole, Indazole. *Inorg. Chem.* **2004**, *43*, 7083–7093. [[CrossRef](#)] [[PubMed](#)]
33. Bruker. *APEX2 & SAINT*; AXS Inc.: Madison, WI, USA, 2004.
34. Sheldrick, G.M. A short history of SHELX. *Acta Crystallogr. Sect. A* **2008**, *64*, 112–122. [[CrossRef](#)] [[PubMed](#)]
35. Farrugia, L.J. WinGX suite for small-molecule single-crystal crystallography. *J. Appl. Crystallogr.* **1999**, *32*, 837–838. [[CrossRef](#)]
36. Spek, A.L. PLATON, an Integrated Tool for the Analysis of the Results of a Single Crystal Structure Determination. *Acta Crystallogr. Sect. A* **1990**, *46*, C34.
37. Nakamoto, K. *Infrared and Raman Spectra of Inorganic and Coordination Compounds*, 5th ed.; Wiley & Sons: New York, NY, USA, 1997.
38. Wallar, B.J.; Lipscomb, J.D. Dioxygen Activation by Enzymes Containing Binuclear Non-Heme Iron Clusters. *Chem. Rev.* **1996**, *96*, 2625–2658. [[CrossRef](#)] [[PubMed](#)]
39. Spackman, M.A.; Jayatilaka, D. Hirshfeld surface analysis. *CrystEngComm* **2009**, *11*, 19–32. [[CrossRef](#)]
40. Timokhin, I.; Pettinari, C.; Marchetti, F.; Pettinari, R.; Condello, F.; Galli, S.; Alegria, E.C.B.A.; Martins, L.M.D.R.S.; Pombeiro, A.J.L. Novel Coordination Polymers with (Pyrazolato)-based Tectons: Catalytic Activity in the Peroxidative Oxidation of Alcohols and Cyclohexane. *Cryst. Growth Des.* **2015**, *15*, 2303–2317. [[CrossRef](#)]
41. Martins, L.M.D.R.S.; de Peixoto Almeida, M.; Carabineiro, S.A.C.; Figueiredo, J.L.; Pombeiro, A.J.L. Heterogenisation of a C-Scorpionate FeII Complex on Carbon Materials for Cyclohexane Oxidation with Hydrogen Peroxide. *ChemCatChem* **2013**, *5*, 3847–3856. [[CrossRef](#)]
42. Sutradhar, M.; Barman, T.R.; Pombeiro, A.J.L.; Martins, L.M.D.R.S. Cu(II) and Fe(III) complexes derived from N-acetylpyrazine-2-carbohydrazide as efficient catalysts towards solvent-free microwave assisted oxidation of alcohols. *Catalysts* **2019**, *9*, 1053. [[CrossRef](#)]

43. Pettinari, C.; Marchetti, F.; Cerquetella, A.; Pettinari, R.; Monari, M.; Leod, T.C.O.M.; Martins, L.M.D.R.S.; Pombeiro, A.J.L. Coordination chemistry of the ( $\eta^6$ -cymene)ruthenium(II) fragment with bis-, tris-, and tetrakis(pyrazol-1-yl)borate ligands: Synthesis, structural, electrochemical and catalytic diastereoselective nitroaldol reaction studies. *Organometallics* **2011**, *30*, 1616–1626. [[CrossRef](#)]
44. Ribeiro, A.P.C.; Martins, L.M.D.R.S.; Hazra, S.; Pombeiro, A.J.L. Catalytic Oxidation of Cyclohexane with Hydrogen Peroxide and a Tetracopper(II) Complex in an Ionic Liquid. *Comptes Rendus Chim.* **2015**, *18*, 758–765. [[CrossRef](#)]
45. Figiel, P.J.; Leskelä, M.; Repo, T. TEMPO-Copper(II) Diimine-Catalysed Oxidation of Benzylic Alcohols in Aqueous Media. *Adv. Synth. Catal.* **2007**, *349*, 1173–1179. [[CrossRef](#)]
46. Karmakar, A.; Soliman, M.M.A.; Alegria, E.C.B.A.; Rúbio, G.M.D.M.; da Guedes Silva, M.F.C.; Pombeiro, A.J.L. A copper-amidocarboxylate based metal organic macrocycle and framework: Synthesis, structure and catalytic activities towards microwave assisted alcohol oxidation and Knoevenagel reactions. *New J. Chem.* **2019**, *43*, 9843–9854. [[CrossRef](#)]



© 2020 by the authors. Licensee MDPI, Basel, Switzerland. This article is an open access article distributed under the terms and conditions of the Creative Commons Attribution (CC BY) license (<http://creativecommons.org/licenses/by/4.0/>).